RESEARCH ARTICLE



Check for updates

Exceptional heat and atmospheric dryness amplified losses of primary production during the 2020 U.S. Southwest hot drought

Matthew P. Dannenberg¹ | Dong Yan^{2,3} | Mallory L. Barnes⁴ | William K. Smith³ | Miriam R. Johnston¹ | Russell L. Scott⁵ | Joel A. Biederman⁵ | John F. Knowles⁶ | Xian Wang³ | Tomer Duman⁷ | Marcy E. Litvak⁷ | John S. Kimball⁸ | A. Park Williams⁹ | Yao Zhang¹⁰

Correspondence

Matthew P. Dannenberg, Department of Geographical and Sustainability Sciences, University of Iowa, Iowa City, IA 52245, IISA

Email: matthew-dannenberg@uiowa.edu

Funding information

National Aeronautics and Space Administration, Grant/Award Number: 80NSSC19K1335 and 80NSSC20K1805; National Science Foundation, Grant/ Award Number: 2131853; Strategic Environmental Research and Development Program, Grant/Award Number: RC18-1322; U.S. Department of Agriculture, Grant/Award Number: 58-0111-17-013 and 58-3050-9-013; University of Iowa

Abstract

Earth's ecosystems are increasingly threatened by "hot drought," which occurs when hot air temperatures coincide with precipitation deficits, intensifying the hydrological, physiological, and ecological effects of drought by enhancing evaporative losses of soil moisture (SM) and increasing plant stress due to higher vapor pressure deficit (VPD). Drought-induced reductions in gross primary production (GPP) exert a major influence on the terrestrial carbon sink, but the extent to which hotter and atmospherically drier conditions will amplify the effects of precipitation deficits on Earth's carbon cycle remains largely unknown. During summer and autumn 2020, the U.S. Southwest experienced one of the most intense hot droughts on record, with recordlow precipitation and record-high air temperature and VPD across the region. Here, we use this natural experiment to evaluate the effects of hot drought on GPP and further decompose those negative GPP anomalies into their constituent meteorological and hydrological drivers. We found a 122 Tg C (>25%) reduction in GPP below the 2015-2019 mean, by far the lowest regional GPP over the Soil Moisture Active Passive satellite record. Roughly half of the estimated GPP loss was attributable to low SM (likely a combination of record-low precipitation and warming-enhanced

This is an open access article under the terms of the Creative Commons Attribution-NonCommercial License, which permits use, distribution and reproduction in any medium, provided the original work is properly cited and is not used for commercial purposes.

© 2022 The Authors. Global Change Biology published by John Wiley & Sons Ltd. This article has been contributed to by US Government employees and their work is in the public domain in the USA.

¹Department of Geographical and Sustainability Sciences, University of Iowa, Iowa City, Iowa, USA

²Information and Data Center, China Renewable Energy Engineering Institute, Beijing, China

³School of Natural Resources and the Environment, University of Arizona, Tucson, Arizona, USA

⁴O'Neill School of Public and Environmental Affairs, Indiana University, Bloomington, Indiana, USA

⁵Southwest Watershed Research Center, Agricultural Research Service, U.S. Department of Agriculture, Tucson, Arizona, USA

⁶Department of Earth and Environmental Sciences, California State University, Chico, California, USA

⁷Department of Biology, University of New Mexico, Albuquerque, New Mexico, USA

⁸Numerical Terradynamic Simulation Group, University of Montana, Missoula, Montana, USA

⁹Department of Geography, University of California, Los Angeles, California, USA

¹⁰Sino-French Institute for Earth System Science, College of Urban and Environmental Sciences, Peking University, Beijing, China

evaporative depletion), but record-breaking VPD amplified the reduction of GPP, contributing roughly 40% of the GPP anomaly. Both air temperature and VPD are very likely to continue increasing over the next century, likely leading to more frequent and intense hot droughts and substantially enhancing drought-induced GPP reductions.

KEYWORDS

drought, drylands, gross primary production (GPP), soil moisture, vapor pressure deficit, warming

1 | INTRODUCTION

Severe and prolonged droughts are among the costliest and deadliest natural disasters (Cook, 2019), causing reduced agricultural productivity (Ault, 2020; Gupta et al., 2020) and extensive vegetation mortality (Allen et al., 2015; Breshears et al., 2005, 2009). Although meteorological droughts occur naturally due to internal variability in the climate system, anthropogenic warming has steadily altered baseline conditions toward higher frequency and intensity of "hot droughts," in which warmer and drier atmospheric conditions coincide with precipitation deficits, substantially exacerbating losses of soil moisture (SM; Williams et al., 2015, 2020) and amplifying deleterious effects on vegetation (Breshears et al., 2005, 2009). As anthropogenic warming continues over the next century, "hot drought" events will likely become a new normal (Bradford et al., 2020; Cook et al., 2015; Diffenbaugh et al., 2015).

Drought-induced reductions in the gross primary production (GPP) of vegetation are major contributors to variation in the terrestrial carbon sink, with arid and semiarid ecosystems contributing much of this variability due to their large spatial extent (~40% of Earth's land surface) and high sensitivity to climate (Ahlström et al., 2015; Poulter et al., 2014). While dryland primary production is predominantly limited by SM availability (Novick et al., 2016; Stocker et al., 2018), vapor pressure deficit (VPD) also limits primary production as plants close stomata to prevent excessive water loss and disruption of xylem water transport (McDowell et al., 2008, 2016; Novick et al., 2016; Roby et al., 2020). Because the saturation vapor pressure of the atmosphere increases

exponentially with temperature, increases in VPD are expected with warming (even if relative humidity were held constant). Anthropogenic warming could therefore compound the effects of drought on GPP through both reduced SM (enhanced by accelerated evaporative losses from hotter and atmospherically drier conditions) and direct physiological responses to high heat and VPD that exacerbate the loss of GPP.

The extended 21st century drought conditions in the U.S. Southwest (hereafter "the Southwest") are among the most extreme in the instrumental record, largely attributable to anthropogenic warming (Williams et al., 2015, 2020) and comparable in severity, extent, and duration to the decades-long "megadroughts" inferred from paleoclimate proxies (Cook et al., 2016; Williams et al., 2020). However, even by recent standards, the summer and autumn drought of 2020 in the Southwest was climatically exceptional (Figure 1). During July through October, typically the wettest time of year in much of the region due to the influence of the North American Monsoon (Adams & Comrie, 1997), roughly 20% of the western United States (areas west of the 100th meridian) received record low precipitation, primarily in the southwestern states of California, Arizona, Nevada, and Utah (Figure 1a). Precipitation deficits of this magnitude would have caused severe drought conditions on their own, but the 2020 drought also coincided with exceptional, record-breaking heat and VPD (Figure 1b,c), consistent with expectations of anthropogenically driven increases in the frequency and intensity of "hot drought" (Bradford et al., 2020; Cook et al., 2015; Diffenbaugh et al., 2015).

Here, we quantify the GPP anomaly during the July-October 2020 hot drought across six drought-affected arid and semiarid

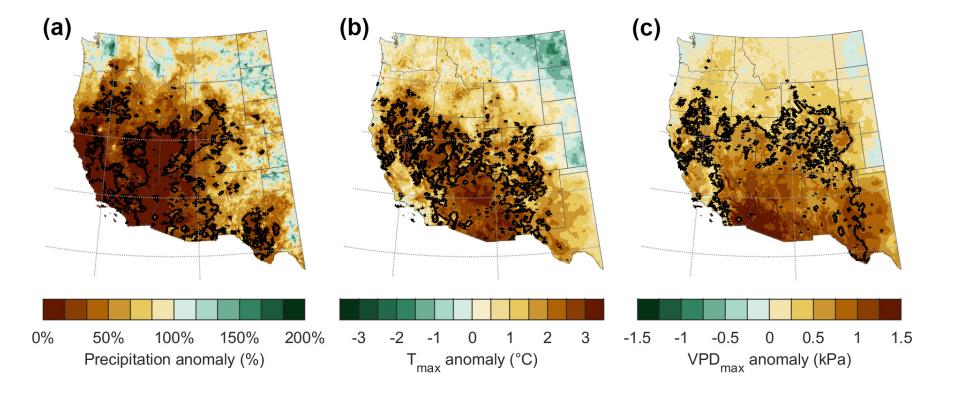


FIGURE 1 (a) Total precipitation anomaly (% of normal), (b) mean maximum daily air temperature anomaly, and (c) mean maximum daily vapor pressure deficit (VPD) anomaly during July-October 2020 relative to a 1981–2010 baseline. Anomalies were derived from 4 km monthly PRISM climate group data (Daly et al., 2008). Areas outlined in black show where July-October precipitation was the lowest on record (a), or air temperature (b) or VPD (c) were the highest on record relative to the full instrumental period (1895–2020)

ecoregions of the Southwest using monthly data from eddy covariance flux towers, optical and microwave satellite observations, and meteorological data. To clarify the mechanisms of primary production loss during hot drought, we use a combination of principal component analysis (PCA), stepwise multiple regression, and scenario differencing to empirically partition the GPP anomaly into components driven by photosynthetically active radiation (PAR), SM, air temperature ($T_{\rm air}$), and VPD. Since the 2020 drought was driven by both record-low precipitation and record-high temperature and VPD, it provides a unique natural experiment to examine two questions:

- 1. How much was GPP in the Southwest reduced by the exceptional 2020 hot drought?
- To what extent did record-breaking T_{air} and VPD amplify drought impacts on GPP?

Because hot droughts are likely to continue increasing in frequency and intensity with further warming, determining the relative balance of these drivers is essential for improving the representation of dryland carbon fluxes in mechanistic models (MacBean et al., 2021) and incorporating climate change into assessments of dryland ecosystem services (Scheiter et al., 2019).

2 | MATERIALS AND METHODS

2.1 | Gross primary production

To assess regional reduction of primary production and decompose those anomalies into their meteorological and hydrological drivers, we used daily 9 km GPP estimates from the Soil Moisture Active Passive (SMAP) L4C product (Jones et al., 2017), which has been operational since April 2015. The SMAP L4C algorithm is based on light-use efficiency theory, in which GPP is proportional to PAR absorbed by the plant canopy (Song et al., 2013). The efficiency with which absorbed PAR is converted to GPP varies by biome and is limited by nonoptimal environmental conditions, with parameters calibrated using global eddy covariance data (Jones et al., 2017). Like many light-use efficiency models, the SMAP L4C model simulates reductions of light-use efficiency in response to sub-optimal air temperature and high VPD, but unlike most prior models, SMAP L4C also includes both root zone (0-1 m depth) SM and frozen-ground response functions based on the SMAP Level 4 Soil Moisture (L4SM) product. SM is a critical driver of canopy structure and physiology in dryland ecosystems (Novick et al., 2016; Smith et al., 2019; Stocker et al., 2018), but prior to SMAP, the limited availability of SM observations at appropriate spatial and temporal scales prevented their widespread use in light-use efficiency models (Smith et al., 2019; Song et al., 2013).

Since SMAP L4C assumes positive responses of GPP to PAR, air temperature, and SM, and negative responses to VPD, the modeled

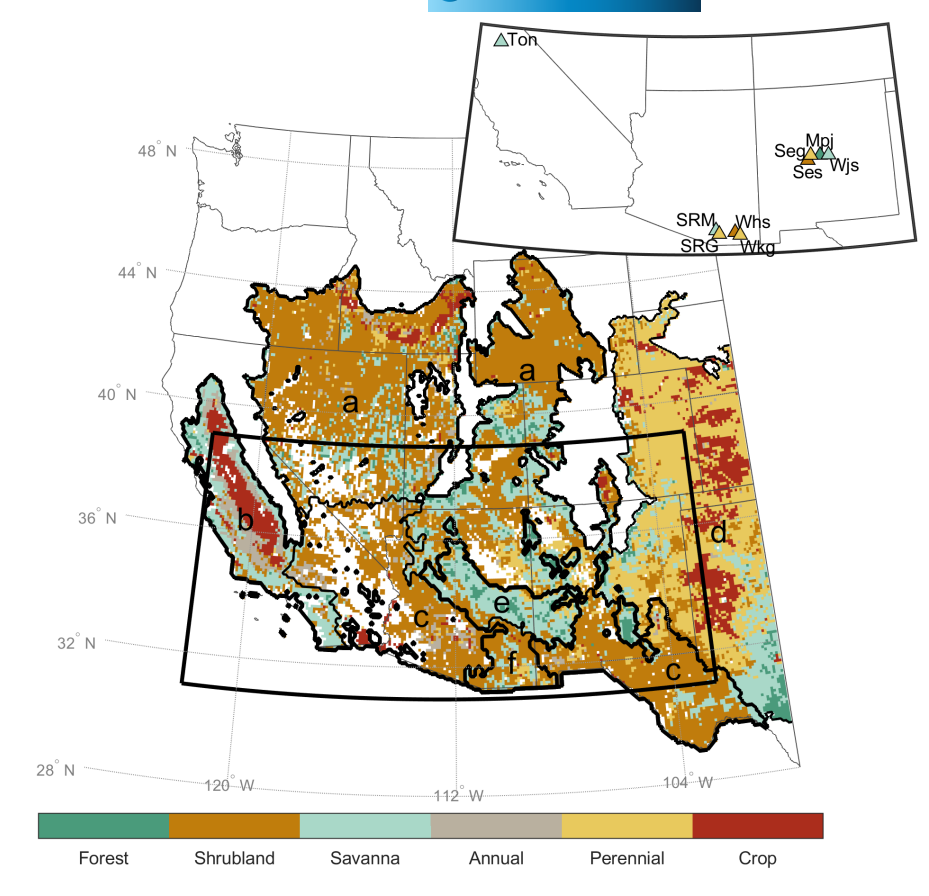
responses of GPP to any given meteorological variable are determined both by: (1) how that variable affects the remotely sensed vegetation index used to estimate light absorption and (2) the a priori assumptions of the model regarding functional responses of vegetation to nonoptimal conditions. For example, if SMAP L4C includes a direct positive response of GPP to SM, then any reduction in SM during the drought will, by definition, negatively force GPP, though the influence of the built-in response functions will be partly mediated by how canopy light absorption responds to drought. To address this partial circularity, we also used two alternative estimates of (or proxies for) GPP that are largely independent of meteorological inputs: eddy covariance estimates of GPP from nine sites distributed across California, Arizona, and New Mexico (Figure 2; Table S1) and the satellite-based Contiguous Solar-Induced Fluorescence (CSIF) product.

Eddy covariance estimates of GPP were derived from halfhourly observations of net ecosystem exchange (NEE) of CO₂. Sudden but temporary changes in NEE, which can arise from either biophysical processes (e.g., sudden changes in turbulence) or instrument errors, were first filtered using a spike detection method applied separately to daytime and nighttime observations (Papale et al., 2006). Using the REddyProc package (Wutzler et al., 2018, 2020) in the R statistical computing environment (R Core Team, 2021), we then used a seasonal friction velocity (u*) filter to exclude observations that occurred during periods of low turbulence; gap-filled the missing half-hourly data using a look-up table based on air temperature, radiation, and VPD; and partitioned the NEE into its component fluxes (GPP and ecosystem respiration) using a nighttime partitioning method (Papale et al., 2006; Reichstein et al., 2005). The half-hourly GPP estimates were then summed to daily total GPP, with monthly GPP averaged from the daily fluxes, excluding months where more than half of the daily estimates were missing.

As an additional independent proxy for GPP, we used estimates of solar-induced fluorescence (SIF) from CSIF (Zhang et al., 2018). SIF represents the light re-emitted from chlorophyll during the light reactions of photosynthesis, and both theory and observations indicate that SIF is correlated with photosynthetic activity and directly linked to both PAR absorbed by the plant canopy and light-use efficiency of vegetation (Porcar-Castell et al., 2014), especially when integrated over relatively long periods at the canopy scale (Magney et al., 2020). Compared with many other vegetation indices, SIF also better captures seasonality and variability of dryland GPP (Smith et al., 2018; Wang et al., 2022), though the linearity of the SIF-GPP relationship may break down under extreme heat and drought (Martini et al., 2022). The CSIF dataset was generated by training and validating a neural network with clear-sky SIF retrievals from the Orbiting Carbon Observatory-2 (OCO-2) and MODIS-derived nadir bidirectional reflectance distribution adjusted surface reflectance (MCD43C4). We aggregated the clear-sky CSIF from its 4-day, 0.05° resolution to monthly, 9-km resolution to match the SMAP SM and GPP data.

Global Change Biology -WILEY 4797

FIGURE 2 Land cover of the study area (derived from the Rangeland Analysis V2 land cover product, with croplands defined using the MODIS MCD12C1 land cover), with six major ecoregions labeled and outlined in black: (a) cold deserts, (b) Mediterranean California, (c) warm deserts, (d) semiarid prairies, (e) Upper Gila Mountains, and (f) Sierra Madre piedmont. The nine AmeriFlux eddy covariance towers used in this study (Table S1) are shown in the inset and color-coded by their dominant land cover. Note that adjacent sites (SRG/SRM, Whs/ Wkg, and seg/Ses) were slightly offset from each other to improve visibility



2.2 | Meteorological data

For regional analysis, we used 9 km monthly root-zone (0–1 meter depth) SM estimates (averaged from daily 0:00 UTC retrievals) from SMAP L4SM (Reichle et al., 2019), which assimilates satellite-observed L-band (1.41 GHz) microwave brightness temperature (sensitive to moisture in the upper layers of the soil and vegetation) into a hydrological model forced with instrumental precipitation observations (Reichle et al., 2019). We also obtained gridded incoming shortwave radiation, minimum and maximum $T_{\rm air}$, and VPD from gridMET (Abatzoglou, 2013), which blends regional reanalysis data with high-resolution surface meteorological data to derive daily meteorological estimates at high spatial resolution (4 km) for the continental United States. We assumed that PAR was a constant fraction of incoming shortwave radiation, estimated mean $T_{\rm air}$ as the average of minimum and maximum air temperatures, and calculated monthly averages from the daily data.

For analysis at the eddy covariance sites, we used tower-measured daily mean $T_{\rm air}$, incoming shortwave radiation, and VPD (all averaged from half-hourly observations). We estimated root-zone (0–30 cm) SM using observations from time domain reflectometry (TDR) probes in the soil profile. Since few of the sites have SM probes below 30 cm, our site-level estimates of root-zone SM are necessarily shallower than the root zone defined by SMAP. The depths of the TDR probes also vary across the nine sites, so we standardized the root-zone SM estimates by taking a multi-layer weighted mean of the TDR probes, where each probe was assumed to represent a distinct

layer of varying depths in the soil profile (Figure S1). Daily meteorological and SM observations were then averaged to monthly scale to match the remaining datasets.

2.3 | Drivers of drought-induced gross primary production anomalies

We assessed the influence of each driver variable on GPP during the 2020 drought by fitting statistical models relating monthly anomalies of the four drivers to monthly GPP anomalies (Humphrey et al., 2021; Jung et al., 2017) and then using scenario differencing to estimate the GPP anomaly attributable to each driver (Huntzinger et al., 2017; Wei et al., 2014). The total GPP anomaly (Δ GPP) can be conceptualized as the sum of the anomalies attributable to each individual driver (Jung et al., 2017):

$$\Delta GPP = \Delta GPP_{PAR} + \Delta GPP_{SM} + \Delta GPP_{Tair} + \Delta GPP_{VPD}, \tag{1}$$

where ΔGPP_x represents the GPP anomaly associated with each driver, x. To partition observed ΔGPP into its constituent parts, we used multiple regression models fit individually for each tower and pixel. To best constrain drought impacts on vegetation productivity, regression models were fit using the full period of record for each individual tower (with varying start years; Table S1) and over the 2015–2020 period for the satellite-based models, where the start year is constrained by the beginning of the SMAP record in April 2015. As predictors in the

regression models, we used each of the four driver variables and their 1-month prior lags (eight total variables). Since these drivers are intercorrelated, we used PCA to reduce the variables to a set of leading components, using only the first n PCs that collectively captured at least 95% of the variance. Prior to the PCA, all driver variables were first converted to deseasonalized monthly z-scores (i.e., standardized anomalies relative to the 2015-2019 mean and standard deviation of each month). Those leading PCs were then used as candidate predictors in stepwise multiple regression models, with monthly GPP anomalies (relative to the 2015-2019 monthly mean GPP) as the response variable. Forward- and backward-stepwise selection (using "stepwiselm" in MATLAB) was performed using the Bayesian information criterion (BIC), starting with linear terms for all predictors, with quadratic terms allowed to enter the model if they passed the minimum criterion for entry (change in BIC<0), and with any terms removed if their inclusion increased the BIC by more than 0.01.

We calibrated the models using only months with $T_{\rm air} > 0$ °C to exclude periods when productivity would be primarily temperatureor energy-limited rather than water limited (typically during winter months at higher elevations and latitudes); to ensure an adequate number of observations for training and assessment, we only analyzed pixels with at least 20 months of $T_{air} > 0$ °C. To estimate model skill and uncertainty, we used bootstrapped model ensembles (100-member ensembles at the gridded scale; 1000-member ensembles at the eddy covariance sites), in which each model was trained by randomly selecting (with replacement) N observations for model calibration, where N is the number of records (i.e., monthly observations) in the full dataset. GPP anomalies were predicted for the entire period of record, and model skill (R^2) was calculated using the random subset of observations that were not selected for calibration of that ensemble member, which on average would be approximately 37% of the observations: $e^{-k/N}$, where k is the number of samples drawn from N observations and, in the case of bootstrapping, k = N. For consistency across the full region, all pixel-level models within a given member of the ensemble were calibrated and validated using the same subset of observational time periods.

We used the calibrated models to estimate the total GPP anomaly expected due to all drivers collectively and to each driver individually using a scenario differencing approach (Table S2; Huntzinger et al., 2017; Wei et al., 2014). Specifically, we simulated GPP anomalies under five scenarios, each of which sequentially allowed one additional driver to vary while holding the others constant at their mean value (which, for the z-score deseasonalization, is always zero; Table S2). GPP anomalies attributable to each driver were then estimated as the difference between the scenario in which that variable was allowed to vary and the previous scenario (Table S2; Equations S1-S4). With a purely linear model, the order in which variables enter the model does not affect the partitioning of Δ GPP. However, when nonlinear terms are included in the model, the variable order has a small, but negligible, effect on the results (e.g., compare Figure S2 to Figure S3). We then estimated the total GPP anomaly attributable to each driver during the 2020 drought by summing the modeled monthly anomalies from Equations S1-S4 over the 4-month

July-October period. Confidence intervals on each term (at the 95% level) were estimated by repeating this procedure with each member of the bootstrapped model ensemble and calculating the 2.5th and 97.5th percentiles across the ensemble.

We calculated mean GPP anomalies (and their confidence intervals) across six arid and semiarid ecoregions of the Southwest (Figure 2; Omernik, 1987), as well as five dominant land cover types derived from the 2020 Rangeland Analysis V2 dataset (Allred et al., 2021; Jones et al., 2018): forest (≥30% tree cover), savanna (10%-30% tree cover), shrubland (≥10% shrub cover and <10% tree cover), annual-dominated grassland, and perennial-dominated grassland (Figure 2). We did the same for croplands in California's Central Valley and in the Great Plains (mostly western Texas and Kansas), both defined with the MODIS land cover product (MCD12C1; Sulla-Menashe et al., 2019). We also calculated the total GPP anomaly (and its component parts from Equations S1-S4) across the whole region by multiplying the GPP anomaly of each pixel by its areal coverage $(9000 \,\mathrm{m} \times 9000 \,\mathrm{m} = 81.000.000 \,\mathrm{m}^2)$ and summing across all pixels. We did the same for each member of the bootstrapped model ensemble and estimated 95% confidence intervals using the 2.5th and 97.5th percentiles across the ensemble.

3 | RESULTS AND DISCUSSION

3.1 | Drought-induced reductions in primary production

Across the dry ecoregions of the Southwest, GPP from the SMAP L4C model was reduced by 122 Tg C (>25% reduction) during the 2020 drought compared with the 2015-2019 average of 452 Tg C (Figure 3a). The total reduction of productivity across the region far exceeded the typical range of variability previously estimated by SMAP L4C (Figure 3a). From 2015-2019, July-October GPP varied from roughly 410-480 Tg C, but GPP fell to only 330 Tg C during the 2020 drought (Figure 3a), <75% of the mean GPP and a far greater reduction than in 2018, when much of the Southwest also experienced moderate to severe drought (Li et al., 2020). This is especially remarkable given that the baseline period itself falls within a multi-decade period of relative dryness compared with 20th century conditions (Williams et al., 2020). This reduction of vegetation production could have direct economic consequences via loss of ecosystem services, including crop production and cattle grazing. For example, the loss of productivity across southwestern shrublands and grasslands was roughly equivalent to that needed to feed 47 million cattle for a month (i.e., animal unit months; Allred et al., 2015).

Estimates of GPP from nine eddy covariance sites, extending as far back as 2001, confirm significant reductions in GPP, with all nine sites experiencing reduced GPP (ranging from 9% to 94% reductions) compared with the 2015–2019 benchmark (Figure 4; Table S3). However, the region-wide SMAP GPP anomaly (–122 Tg C) likely underestimates the true effect of the 2020 hot drought: across the nine eddy covariance sites, the SMAP L4C model substantially

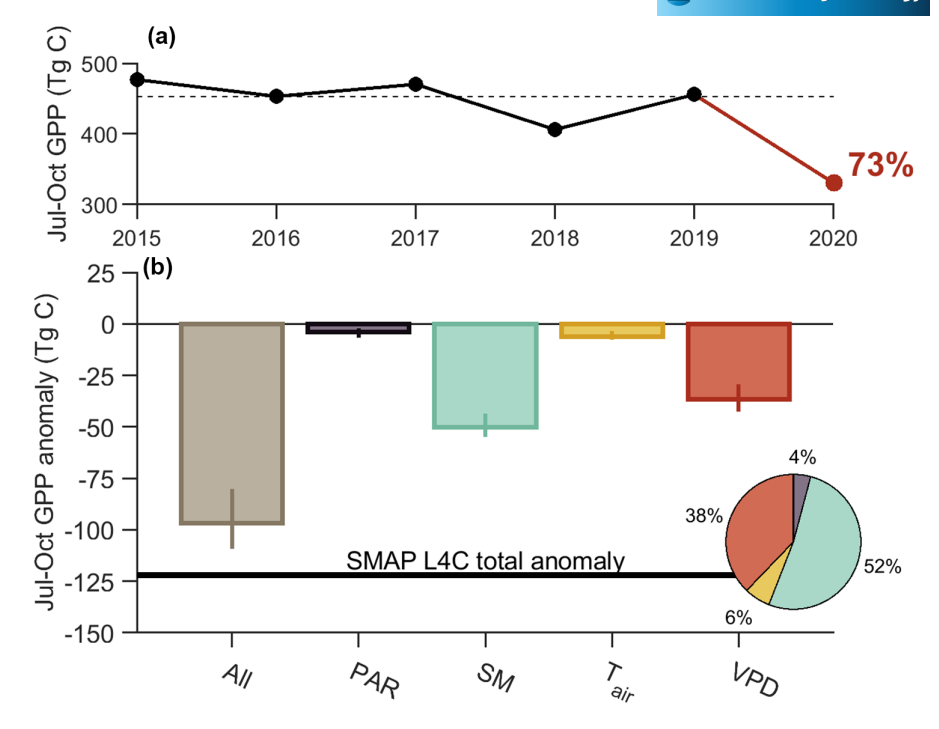


FIGURE 3 (a) Total July-October GPP across the Southwest over the SMAP record. The dashed line shows the overall mean July-October GPP across the region from 2015–2019, and red text shows the 2020 GPP as a percentage of that mean (i.e., regional GPP in 2020 was 73% of the 2015–2019 mean GPP). (b) Overall GPP anomalies across all six ecoregions during July-October 2020 attributable to each driver (bars), relative to a 2015–2019 baseline, and the proportion of the modeled decline in GPP attributable to each individual driver (pie chart). The horizontal black line shows the total SMAP-based July-October 2020 GPP anomaly, and the colored bars show the modeled anomalies (with 95% confidence intervals from the bootstrapped model ensemble) based on all variables (brown) and each variable individually: PAR (dark purple), soil moisture (green), air temperature (yellow), and VPD (red)

underestimated the GPP anomaly relative to the tower-measured GPP by about 40% on average (Figure S4; Tables S3 and S4). Although this could partly reflect scale mismatches between SMAP (81 km² pixel) and the eddy covariance footprint (~1 km²), it is consistent with widespread, systematic underestimation of interannual carbon flux variability by remote sensing in dryland ecosystems (Biederman et al., 2017; Smith et al., 2018; Stocker et al., 2019), highlighting a need to improve representation of extreme events in remote-sensing models.

The 2020 GPP was by far the lowest observed by SMAP in all ecoregions except Mediterranean California, where negative GPP anomalies were comparable with those observed in 2018 (Figure 5). Likewise, all land-cover types experienced substantial reductions in GPP during the 2020 drought compared with their 2015-2019 means (Figure S5), ranging from 10% reductions (croplands in the Central Valley) to 33% reductions (shrubland). The drought-induced reductions of productivity were particularly concentrated in the relatively productive semiarid prairies and Sierra Madre piedmont, where GPP anomalies averaged roughly -90 g C m⁻² during the 2020 drought, corresponding to 27% and 40% reductions (respectively) in GPP relative to their July-October means (Figure 5e,g). The 2020 drought reduced GPP of warm and cold deserts by roughly 40-45 g C m⁻² compared with the 2015–2019 mean (Figure 5b,d), with warm deserts losing nearly 40% of their mean productivity. Of the six ecoregions, the GPP of Mediterranean California was least affected,

with anomalies averaging $-27 \, \mathrm{g} \, \mathrm{C} \, \mathrm{m}^{-2}$ (Figure 5c), but summer and early autumn precipitation provides only a small portion of overall water supply in this region, so much of the vegetation productivity either occurs outside of the July–October period or is supplemented by irrigation in the Central Valley.

3.2 | Drivers of reduced primary production during drought

While most of the reduced GPP during the 2020 Southwest drought was attributable to low SM, those reductions were significantly amplified by high VPD (Figure 3b). The model based on all four factors (PAR, SM, $T_{\rm air}$, and VPD) underestimated the observed GPP anomaly by about 25 Tg C (Figure 3b), suggesting either that unresolved variance in the model (Figure S6) resulted in an underestimation of extremes or that the drought was severe enough to cause nonlinear or structural change that was not captured in the model. However, of the –97 Tg C (95% confidence interval: [–109, –80] Tg C) GPP anomaly predicted by the full model (ΔGPP_{All}), –50 [–55, –44] Tg C was attributable to SM effects (52% of the anomaly) and –37 [–42, –29] Tg C was attributable to VPD effects (38% of the anomaly; Figure 3b), indicating that drought effects on GPP were substantially and significantly amplified by record-breaking VPD. High $T_{\rm air}$ also had a small negative effect on GPP during the drought (–6 [–8, –3] Tg C), though

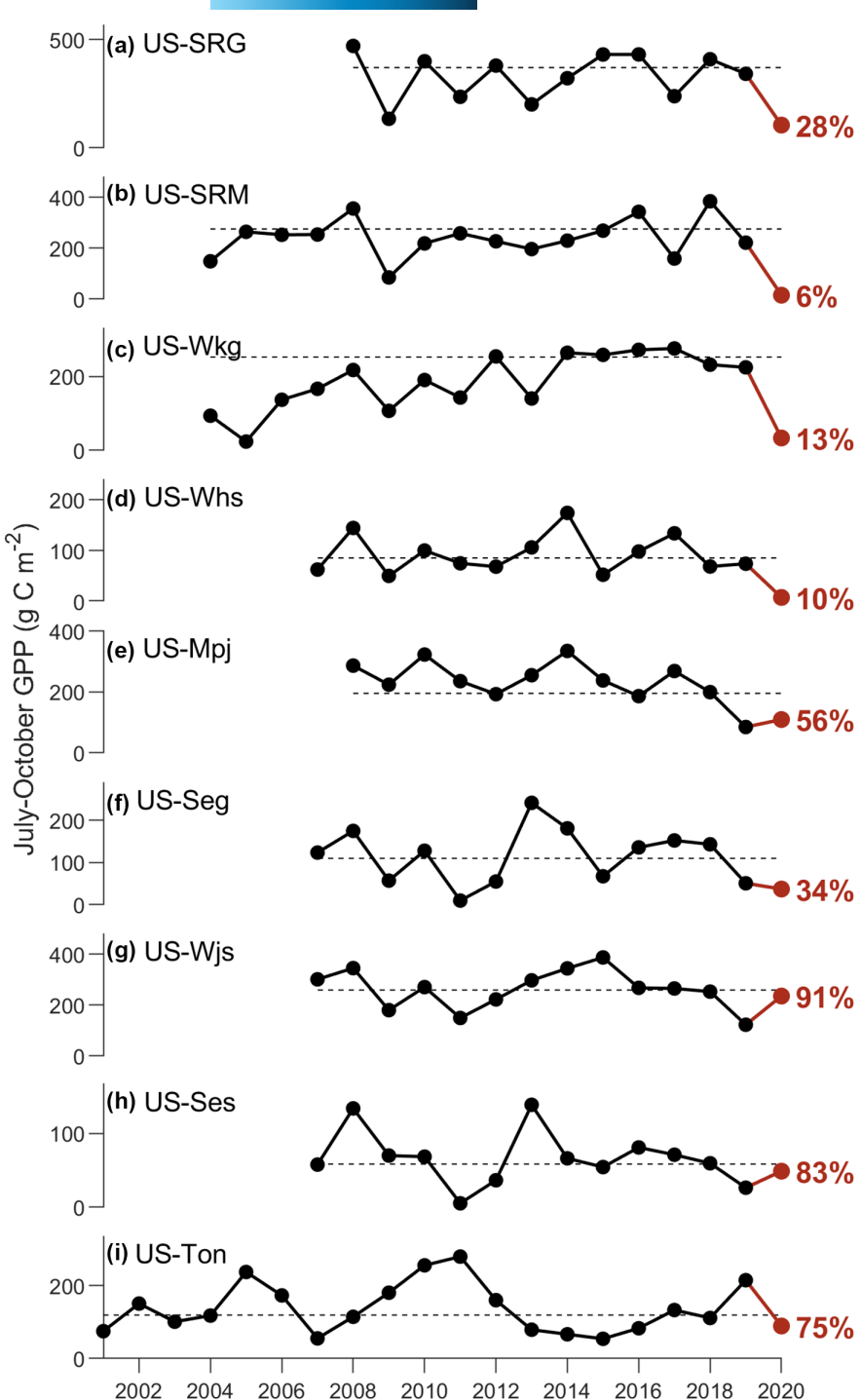


FIGURE 4 Time series of July-October gross primary production (GPP) at each flux tower: (a) Santa Rita Grassland (US-SRG), (b) Santa Rita Mesquite (US-SRM), (c) Walnut Gulch Kendall Grasslands (US-Wkg), (d) Walnut Gulch Lucky Hills Shrubland (US-Whs), (e) Mountainair Pinyon-Juniper Woodland (US-Mpj), (f) Sevilleta Grassland (US-Seg), (g) Willard Juniper Savanna (US-Wjs), (h) Sevilleta Shrubland (US-Ses), and (i) Tonzi Ranch (US-Ton). Horizontal dashed lines show the mean 2015–2019 July-October GPP, and red text shows the 2020 GPP as a percentage of that mean

it likely also had large indirect effects through increased saturation vapor pressure. This is consistent with recent work showing widespread evidence for increasing negative GPP extremes due to hot drought (Gampe et al., 2021).

The amplification of soil-moisture induced reductions in GPP by high VPD occurred across most of the individual ecoregions (Figure 6a-f and Figure S7; Table S5) and land cover types (Figure 6g-m), with most of the GPP reduction attributable to low SM (~50%-60% of the modeled GPP anomalies) but substantially amplified by high VPD (~40% of the modeled GPP anomalies). Land

cover types with substantial woody components (forest, savanna, and shrubland) experienced reductions in GPP of roughly 50–60 g C m $^{-2}$ during the drought, driven mostly by low SM and enhanced by high VPD (Figure 6g–i). In Mediterranean California, however, most of the relatively small GPP anomaly was attributable to high VPD (~90% of the modeled anomaly), with both SM and $T_{\rm air}$ causing smaller reductions (~15%–25% each of the modeled anomaly) and with PAR partly offsetting losses of GPP (Figure 6b). The relatively low SM effect in this region could be due to (i) the summer-dry Mediterranean climate (opposite to the summer-wet majority of

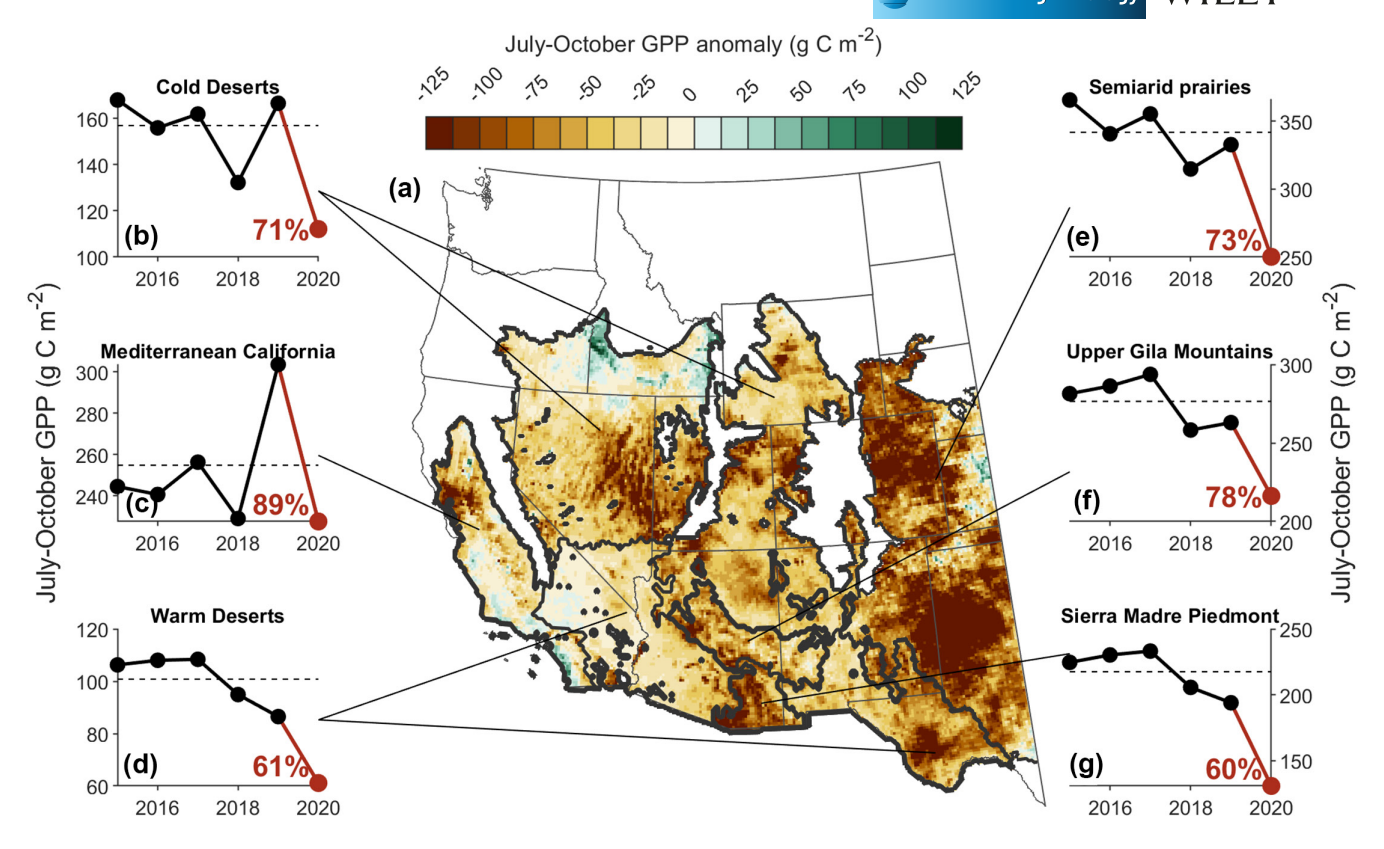


FIGURE 5 (a) Map of SMAP-based gross primary production (GPP) anomalies during the July-October 2020 drought relative to a 2015–2019 baseline, and (b–g) time series of annual July-October SMAP GPP for each ecoregion. Dashed horizontal lines indicate the mean 2015–2019 July-October GPP of each ecoregion, and red numbers show the 2020 July-October GPP as a percentage of the 2015–2019 mean in each ecoregion

the region) leading to consistently low baseline summer SM even under non-drought conditions, making the SM anomaly during the 2020 drought comparable with normal conditions for that time of year; (ii) the presence of deep-rooted trees capable of accessing stores of deep subsurface moisture that buffer against drought (McCormick et al., 2021; Miller et al., 2010); or (iii) irrigation in the Central Valley, which supplements the SM but does not fully alleviate the negative effects of VPD on plant function. For example, the 2020 GPP was ~50 g C m⁻² below average in Central Valley croplands (Figure 6I and Figure S5f), mostly attributable to high VPD. By contrast, croplands in the Great Plains had greater reductions of productivity during the drought (exceeding –100 g C m⁻²), mostly due to low SM (Figure 6m), possibly reflecting more dependence on summer rain.

GPP estimates from the eddy covariance sites confirm the amplification of drought-induced loss of productivity by exceptionally high heat and VPD (Figures S2 and S3). Productivity decreased at all nine sites during the 2020 drought, with anomalies ranging from -10 to $-265\,\mathrm{g}$ C m $^{-2}$ (Figure S2; Table S3). All sites experienced significant reductions in GPP due to low SM, and those losses were significantly (p<.05) exacerbated by high VPD at seven sites and, to a lesser extent, by high T_{air} at six sites. The relative effects of SM versus VPD based on the SMAP L4C model were generally similar

to eddy covariance estimates, though SMAP either overestimated the VPD effect or underestimated the SM effect at several sites (compare Figures S2 and S8 and Tables S3 and S4). This agreement corroborates the amplifying role of VPD during drought across the region and suggests that the effects observed by SMAP L4C are not mere artifacts of the model structure and assumptions. Independent, machine-learning-based estimates of SIF derived from MODIS surface reflectance (CSIF) also show reductions in plant activity attributable to both low SM (64% of the anomaly) and high VPD (27% of the anomaly; Figures S7c,d, S9-S11). However, the relative strength of the VPD effect was smaller than in SMAP L4C and most eddy covariance sites, which may reflect deficiencies in the ability of satellite optical reflectance to capture some of the underlying physiological responses to drought, leading to underestimates of drought-induced loss of productivity. Given that the primary vegetation influences on surface reflectance are green leaf area and canopy structure, which vary on relatively slow time scales comparable with variation of SM, reflectance-based indices may not capture fast physiological responses to atmospheric conditions. This may be especially true in dryland ecosystems, where GPP can become decoupled from vegetation greenness during drought when many woody plants can retain leaves even under severe moisture stress (Smith et al., 2018, 2019; Yan et al., 2019).

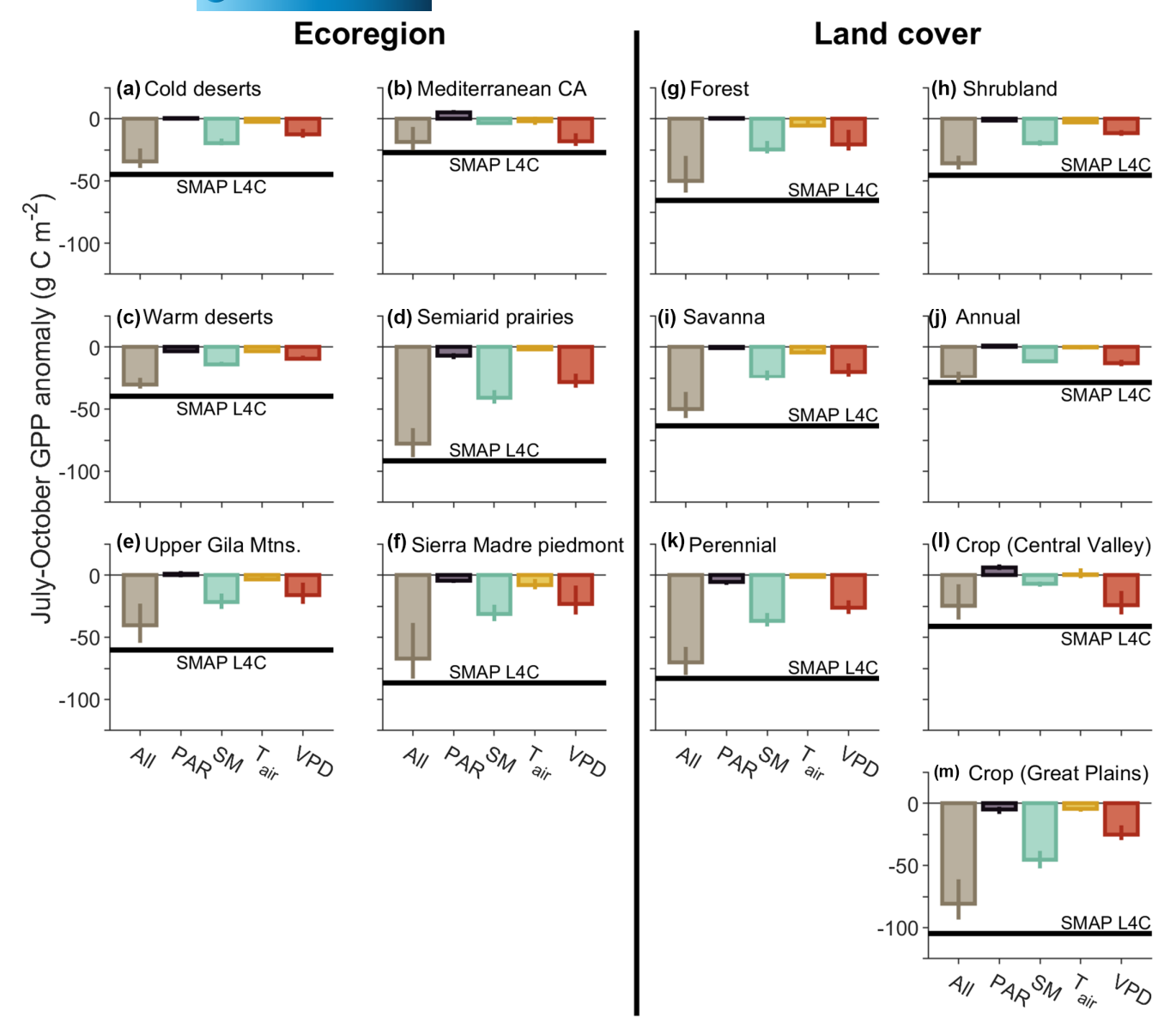


FIGURE 6 Observed and modeled GPP anomalies, and attribution to each of the four driver variables, for each ecoregion (a–f) and land-cover type (g–m). Given distinct management regimes and climates, croplands are separated geographically into Central Valley croplands (I) and croplands in the Great Plains (m). The horizontal black lines show the SMAP-based July-October 2020 GPP anomalies (relative to the 2015–2019 baseline), and the colored bars show the modeled anomalies (with 95% confidence interval) based on all variables (brown) and each variable individually: PAR (dark purple), soil moisture (green), air temperature (yellow), and VPD (red)

4 | CONCLUSIONS

Air temperature and VPD have increased substantially across the U.S. Southwest over the past century (Ficklin & Novick, 2017; Williams et al., 2020; Zhang, Biederman, et al., 2021), and further increases over the next century are very likely (Cook et al., 2014; Ficklin & Novick, 2017). As a result, meteorological droughts are superimposed on a hotter and atmospherically drier background climate (Zhou, Williams, et al., 2019), which could substantially amplify the impacts of drought on ecosystems, both directly via physiological impacts on vegetation (Grossiord et al., 2020) and indirectly through greater soil water evaporation (Williams et al., 2020). In 2020, widespread reductions in GPP throughout the U.S. Southwest

coincided with a period of exceptional, record-breaking hot drought, consistent with expectations for droughts in a warmer future. Here, we show that the negative effects of SM on GPP during drought were substantially amplified by the high VPD that is characteristic of a hot drought.

The direct effects of VPD on GPP come largely via stomatal and plant hydraulic responses. High VPD induces stomatal closure in part to prevent excessive water loss and desiccation of plant leaves but at the cost of reducing carbon uptake (Novick et al., 2016). However, in some extreme cases, high air temperature can actually result in increased stomatal conductance as plants attempt to shed excess heat via transpiration, resulting in rapid desiccation and elevated mortality risk (Marchin et al., 2022). High heat and VPD also increase

the risk of hydraulic failure (McDowell et al., 2008) and shorten the time to mortality (Adams et al., 2009; Allen et al., 2015; Duan et al., 2018), with tall trees potentially being especially vulnerable (McDowell & Allen, 2015). High VPD also indirectly affects GPP by increasing losses of SM (Williams et al., 2020). For example, anthropogenic trends in air temperature and humidity accounted for about 20%-25% of SM losses during the 2012-2014 California drought (Williams et al., 2015) and nearly 50% of SM losses during the extended 2000-2018 drought in the Southwest (Williams et al., 2020). Because high air temperature and VPD increase atmospheric evaporative demand, much of the reduced SM during the 2020 Southwest drought was likely enhanced by evaporative drying of soils. The large observed reductions in GPP across the U.S. Southwest during the July-October 2020 drought, therefore, likely represent an integrated response to the forcings of precipitation deficit, extreme heat, and high VPD. Especially when combined with recent and projected changes in precipitation variability (Dannenberg et al., 2019; Pendergrass et al., 2017; Zhang, Biederman, et al., 2021), increasing frequency and severity of "hot drought" conditions under warming could negatively affect ecosystem productivity from both ends of the soil-plant-atmosphere continuum: not only does warming exacerbate losses of SM, but direct responses of plant hydraulics and physiology to high VPD restrict canopy conductance and carbon uptake.

Because our regression-based modeling approach included both SM and VPD as predictors, we expect that our quantification of the VPD and SM influences on the GPP anomaly mostly captured direct rather than indirect effects. However, while we attempted to separate the effects of SM, air temperature, and VPD, they are all coupled and difficult to disentangle, especially at longer time scales (Humphrey et al., 2021; Novick et al., 2016; Zhou, Zhang, et al., 2019). In addition to the influence of VPD on SM, for example, SM affects VPD: decreased SM reservoirs depress evaporative cooling, which results in higher surface air temperature, lower humidity, and, consequently, higher VPD (Seneviratne et al., 2013; Yin et al., 2014; Zhou, Williams, et al., 2019). Our combined use of deseasonalization (which reduces the correlation between each variable resulting from similarities in their seasonal cycles), PCA, and stepwise variable selection was designed to mitigate uncertainties arising from their collinearity, though we note that varying model structures across sites resulting from the combined use of PCA and stepwise selection could impose their own uncertainties on the pooled anomaly attribution. The SMAP GPP estimates could also overestimate VPD effects due to the inclusion of direct, a priori VPD responses in the algorithm. However, estimates of GPP from both eddy covariance and CSIF, which are largely independent of meteorological inputs and do not assume any functional relationship between GPP and meteorological drivers, also show large negative effects of VPD on carbon uptake during drought, albeit of a slightly smaller magnitude than SMAP L4C.

Decreased GPP associated with hot drought may be partly offset by expected increases in plant water-use efficiency due to elevated atmospheric CO₂ (De Kauwe et al., 2021; Walker et al., 2021). Anthropogenic increases in atmospheric CO_2 have enhanced both the global GPP and the amount of carbon taken up per unit water loss (water-use efficiency). However, the extent to which enhanced CO_2 will reduce plant water use and ameliorate water stress during drought is unclear and contested (De Kauwe et al., 2021), with some evidence suggesting that CO_2 fertilization has only a minimal benefit during drought (Obermeier et al., 2017; Reich et al., 2014; Walker et al., 2021) and that increases in leaf area from CO_2 fertilization can actually increase plant susceptibility to drought (Duan et al., 2018; Zhang, Keenan, & Zhou, 2021).

ACKNOWLEDGEMENTS

This research was supported by the NASA SMAP Science Team (grant number 80NSSC20K1805), the Strategic Environmental Research and Development Program (SERDP; project number RC18-1322), NSF EPSCoR (grant number 2131853), the Future Investigators in NASA Earth and Space Science and Technology (FINESST) program (grant number 80NSSC19K1335), and the scholar-in-residence program at the University of Iowa's Public Policy Center. W.K.S. also acknowledges support from the U.S. Department of Agriculture (cooperative agreement 58-3050-9-013 and 58-0111-17-013). We thank three anonymous reviewers for constructive comments that improved the manuscript.

CONFLICT OF INTEREST

The authors have no conflicts of interest to declare.

DATA AVAILABILITY STATEMENT

All data are publicly available. SMAP L4C and L4SM are available at the National Snow and Ice Data Center (https://nsidc.org/data/spl4cmdl and https://nsidc.org/data/SPL4SMAU/versions/6, respectively). Eddy covariance data can be obtained from AmeriFlux (https://ameriflux.lbl.gov/). CSIF data are available at https://osf. io/8xqy6/. Climate data are available from gridMET (https://www.climatologylab.org/gridmet.html) and the PRISM Climate Group at Oregon State University (https://prism.oregonstate.edu/). MATLAB code for the analysis is available at https://github.com/mpdannenberg/southwest-drought-2020.

ORCID

Matthew P. Dannenberg https://orcid.
org/0000-0002-6518-4897

Joel A. Biederman https://orcid.org/0000-0002-1831-461X

Xian Wang https://orcid.org/0000-0003-0018-2679

Marcy E. Litvak https://orcid.org/0000-0002-4255-2263

Yao Zhang https://orcid.org/0000-0002-7468-2409

REFERENCES

Abatzoglou, J. T. (2013). Development of gridded surface meteorological data for ecological applications and modelling. *International Journal of Climatology*, 33(1), 121–131. https://doi.org/10.1002/joc.3413

Adams, D. K., & Comrie, A. C. (1997). The north American monsoon. Bulletin of the American Meteorological Society, 78(10), 2197-2213.

- https://doi.org/10.1175/1520-0477(1997)078<2197:TNAM>2.0.
- Adams, H. D., Guardiola-Claramonte, M., Barron-Gafford, G. A., Villegas, J. C., Breshears, D. D., Zou, C. B., Troch, P. A., & Huxman, T. E. (2009). Temperature sensitivity of drought-induced tree mortality portends increased regional die-off under global-change-type drought. *Proceedings of the National Academy of Sciences*, 106(17), 7063–7066. https://doi.org/10.1073/pnas.0901438106
- Ahlström, A., Raupach, M. R., Schurgers, G., Smith, B., Arneth, A., Jung, M., Reichstein, M., Canadell, J. G., Friedlingstein, P., Jain, A. K., Kato, E., Poulter, B., Sitch, S., Stocker, B. D., Viovy, N., Wang, Y. P., Wiltshire, A., Zaehle, S., & Zeng, N. (2015). The dominant role of semi-arid ecosystems in the trend and variability of the land CO2 sink. *Science*, 348(6237), 895–899. https://doi.org/10.1002/2015JA021022
- Allen, C. D., Breshears, D. D., & McDowell, N. G. (2015). On underestimation of global vulnerability to tree mortality and forest die-off from hotter drought in the Anthropocene. *Ecosphere*, 6(8), 129. https://doi.org/10.1890/ES15-00203.1
- Allred, B. W., Bestelmeyer, B. T., Boyd, C. S., Brown, C., Davies, K. W., Duniway, M. C., Ellsworth, L. M., Erickson, T. A., Fuhlendorf, S. D., Griffiths, T. V., Jansen, V., Jones, M. O., Karl, J., Knight, A., Maestas, J. D., Maynard, J. J., McCord, S. E., Naugle, D. E., Starns, H. D., ... Uden, D. R. (2021). Improving Landsat predictions of rangeland fractional cover with multitask learning and uncertainty. Methods in Ecology and Evolution, 12(5), 841–849. https://doi.org/10.1111/2041-210X.13564
- Allred, B. W., Smith, W. K., Twidwell, D., Haggerty, J. H., Running, S. W., Naugle, D. E., & Fuhlendorf, S. D. (2015). Ecosystem services lost to oil and gas in North America. *Science*, 348(6233), 401–402. https://doi.org/10.1126/science.aaa4785
- Ault, T. R. (2020). On the essentials of drought in a changing climate. Science, 368, 256–260.
- Biederman, J. A., Scott, R. L., Bell, T. W., Bowling, D. R., Dore, S., Garatuza-Payan, J., Kolb, T. E., Krishnan, P., Krofcheck, D. J., Litvak, M. E., Maurer, G. E., Meyers, T. P., Oechel, W. C., Papuga, S. A., Ponce-Campos, G. E., Rodriguez, J. C., Smith, W. K., Vargas, R., Watts, C. J., ... Goulden, M. L. (2017). CO2 exchange and evapotranspiration across dryland ecosystems of southwestern North America. Global Change Biology, 23(10), 4204–4221. https://doi.org/10.1111/gcb.13686
- Bradford, J. B., Schlaepfer, D. R., Lauenroth, W. K., & Palmquist, K. A. (2020). Robust ecological drought projections for drylands in the 21st century. Global Change Biology, 26(7), 3906–3919. https://doi. org/10.1111/gcb.15075
- Breshears, D. D., Cobb, N. S., Rich, P. M., Price, K. P., Allen, C. D., Balice, R. G., Romme, W. H., Kastens, J. H., Floyd, M. L., Belnap, J., Anderson, J. J., Myers, O. B., & Meyer, C. W. (2005). Regional vegetation die-off in response to global-change-type drought. Proceedings of the National Academy of Sciences of the United States of America, 102(42), 15144–15148. https://doi.org/10.1073/pnas.0505734102
- Breshears, D. D., Myers, O. B., Meyer, C. W., Barnes, F. J., Zou, C. B., Allen, C. D., McDowell, N. G., & Pockman, W. T. (2009). Tree die-off in response to global change-type drought: Mortality insights from a decade of plant water potential measurements. Frontiers in Ecology and the Environment, 7(4), 185–189. https://doi. org/10.1890/080016
- Cook, B. I. (2019). Drought: An interdisciplinary perspective. Columbia University Press.
- Cook, B. I., Ault, T. R., & Smerdon, J. E. (2015). Unprecedented 21st century drought risk in the American southwest and Central Plains. *Science Advances*, 1, e1400082. https://doi.org/10.1126/sciadv.1400082
- Cook, B. I., Cook, E. R., Smerdon, J. E., Seager, R., Williams, A. P., Coats, S., Stahle, D. W., & Díaz, J. V. (2016). North American megadroughts

- in the common era: Reconstructions and simulations. Wiley Interdisciplinary Reviews: Climate Change, 7(3), 411–432. https://doi.org/10.1002/wcc.394
- Cook, B. I., Smerdon, J. E., Seager, R., & Coats, S. (2014). Global warming and 21st century drying. *Climate Dynamics*, 43, 2607–2627. https://doi.org/10.1007/s00382-014-2075-v
- Daly, C., Halbleib, M., Smith, J. I., Gibson, W. P., Doggett, M. K., Taylor, G. H., Curtis, J., & Pasteris, P. P. (2008). Physiographically sensitive mapping of climatological temperature and precipitation across the conterminous United States. *International Journal of Climatology*, 28, 2031–2064. https://doi.org/10.1002/joc.1688
- Dannenberg, M. P., Wise, E. K., & Smith, W. K. (2019). Reduced tree growth in the semiarid United States due to asymmetric responses to intensifying precipitation extremes. *Science Advances*, 5(10), eaaw0667. https://doi.org/10.1126/sciadv.aaw0667
- De Kauwe, M. G., Medlyn, B. E., & Tissue, D. T. (2021). To what extent can rising [CO2] ameliorate plant drought stress? *New Phytologist*, 231(6), 2118–2124. https://doi.org/10.1111/nph.17540
- Diffenbaugh, N. S., Swain, D. L., & Touma, D. (2015). Anthropogenic warming has increased drought risk in California. *Proceedings of the National Academy of Sciences*, 112(13), 3931–3936. https://doi.org/10.1073/pnas.1422385112
- Duan, H., Chaszar, B., Lewis, J. D., Smith, R. A., Huxman, T. E., & Tissue, D. T. (2018). CO₂ and temperature effects on morphological and physiological traits affecting risk of drought-induced mortality. *Tree Physiology*, 38(8), 1138–1151. https://doi.org/10.1093/treephys/tpy037
- Ficklin, D. L., & Novick, K. A. (2017). Historic and projected changes in vapor pressure deficit suggest a continental-scale drying of the United States atmosphere. *Journal of Geophysical Research*, 122(4), 2061–2079. https://doi.org/10.1002/2016JD025855
- Gampe, D., Zscheischler, J., Reichstein, M., O'Sullivan, M., Smith, W. K., Sitch, S., & Buermann, W. (2021). Increasing impact of warm droughts on northern ecosystem productivity over recent decades. Nature Climate Change, 11(9), 772-779. https://doi.org/10.1038/s41558-021-01112-8
- Grossiord, C., Buckley, T. N., Cernusak, L. A., Novick, K. A., Poulter, B., Siegwolf, R. T. W., Sperry, J. S., & McDowell, N. G. (2020). Plant responses to rising vapor pressure deficit. *New Phytologist*, 226(6), 1550–1566. https://doi.org/10.1111/nph.16485
- Gupta, A., Rico-Medina, A., & Caño-Delgado, A. I. (2020). The physiology of plant responses to drought. *Science*, 368, 266–269.
- Humphrey, V., Berg, A., Ciais, P., Gentine, P., Jung, M., Reichstein, M., Seneviratne, S. I., & Frankenberg, C. (2021). Soil moisture-atmosphere feedback dominates land carbon uptake variability. Nature, 592(7852), 65-69. https://doi.org/10.1038/s41586-021-03325-5
- Huntzinger, D. N., Michalak, A. M., Schwalm, C., Ciais, P., King, A. W., Fang, Y., Schaefer, K., Wei, Y., Cook, R. B., Fisher, J. B., Hayes, D., Huang, M., Ito, A., Jain, A. K., Lei, H., Lu, C., Maignan, F., Mao, J., Parazoo, N., ... Zhao, F. (2017). Uncertainty in the response of terrestrial carbon sink to environmental drivers undermines carbon-climate feedback predictions. *Scientific Reports*, 7, 4765. https://doi.org/10.1038/s41598-017-03818-2
- Jones, L. A., Kimball, J. S., Reichle, R. H., Madani, N., Glassy, J., Ardizzone, J. V., Colliander, A., Cleverly, J., Desai, A. R., Eamus, D., Euskirchen, E. S., Hutley, L., Macfarlane, C., & Scott, R. L. (2017). The SMAP level 4 carbon product for monitoring ecosystem land-atmosphere CO2 exchange. *IEEE Transactions on Geoscience and Remote Sensing*, 55(11), 6517–6532. https://doi.org/10.1109/TGRS.2017.2729343
- Jones, M. O., Allred, B. W., Naugle, D. E., Maestas, J. D., Donnelly, P., Metz, L. J., Karl, J., Smith, R., Bestelmeyer, B., Boyd, C., Kerby, J. D., & McIver, J. D. (2018). Innovation in rangeland monitoring: Annual, 30 m, plant functional type percent cover maps for U.S. rangelands, 1984–2017. Ecosphere, 9(9), e02430. https://doi.org.10.1002/ecs2.2430

- Jung, M., Reichstein, M., Schwalm, C. R., Huntingford, C., Sitch, S., Ahlström, A., Arneth, A., Camps-Valls, G., Ciais, P., Friedlingstein, P., Gans, F., Ichii, K., Jain, A. K., Kato, E., Papale, D., Poulter, B., Raduly, B., Rödenbeck, C., Tramontana, G., ... Zeng, N. (2017). Compensatory water effects link yearly global land CO2 sink changes to temperature. *Nature*, 541(7638), 516-520. https://doi. org/10.1038/nature20780
- Li, X., Xiao, J., Kimball, J. S., Reichle, R. H., Scott, R. L., Litvak, M. E., Bohrer, G., & Frankenberg, C. (2020). Synergistic use of SMAP and OCO-2 data in assessing the responses of ecosystem productivity to the 2018 U.S. drought. *Remote Sensing of Environment*, 251(March), 112062. https://doi.org/10.1016/j.rse.2020.112062
- MacBean, N., Scott, R. L., Biederman, J. A., Peylin, P., Kolb, T., Litvak, M. E., Krishnan, P., Meyers, T. P., Arora, V. K., Bastrikov, V., Goll, D., Lombardozzi, D. L., Nabel, J. E. M. S., Pongratz, J., Sitch, S., Walker, A. P., Zaehle, S., & Moore, D. J. P. (2021). Dynamic global vegetation models underestimate net CO2 flux mean and interannual variability in dryland ecosystems. *Environmental Research Letters*, 16(9), 094023. https://doi.org/10.1088/1748-9326/ac1a38
- Magney, T. S., Barnes, M. L., & Yang, X. (2020). On the covariation of chlorophyll fluorescence and photosynthesis across scales. *Geophysical Research Letters*, 47(23), e2020GL091098. https://doi.org/10.1029/2020GL091098
- Marchin, R. M., Backes, D., Ossola, A., Leishman, M. R., Tjoelker, M. G., & Ellsworth, D. S. (2022). Extreme heat increases stomatal conductance and drought-induced mortality risk in vulnerable plant species. Global Change Biology, 28, 1133–1146. https://doi.org/10.1111/gcb.15976
- Martini, D., Sakowska, K., Wohlfahrt, G., Pacheco-Labrador, J., van der Tol, C., Porcar-Castell, A., Magney, T. S., Carrara, A., Colombo, R., El-Madany, T. S., Gonzalez-Cascon, R., Pilar Martín, M., Julitta, T., Moreno, G., Rascher, U., Reichstein, M., Rossini, M., & Migliavacca, M. (2022). Heatwave breaks down the linearity between suninduced fluorescence and gross primary production. New Phytologist, 233(6), 2415–2428. https://doi.org/10.1111/nph.17920
- McCormick, E. L., Dralle, D. N., Hahm, W. J., Tune, A. K., Schmidt, L. M., Chadwick, K. D., & Rempe, D. M. (2021). Widespread woody plant use of water stored in bedrock. *Nature*, 597(7875), 225–229. https://doi.org/10.1038/s41586-021-03761-3
- McDowell, N. G., & Allen, C. D. (2015). Darcy's law predicts widespread forest mortality under climate warming. *Nature Climate Change*, 5(7), 669–672. https://doi.org/10.1038/nclimate2641
- McDowell, N. G., Pockman, W. T., Allen, C. D., Breshears, D. D., Cobb, N., Kolb, T., Plaut, J., Sperry, J., West, A., Williams, D. G., & Yepez, E. A. (2008). Mechanisms of plant survival and mortality during drought: Why do some plants survive while others succumb to drought? New Phytologist, 178(4), 719–739.
- McDowell, N. G., Williams, A. P., Xu, C., Pockman, W. T., Dickman, L. T., Sevanto, S., Pangle, R., Limosin, J., Plaut, J., Mackay, D. S., Ogee, J., Domec, J. C., Allen, C. D., Fisher, R. A., Jiang, X., Muss, J. D., Breshears, D. D., Rauscher, S. A., & Koven, C. (2016). Multi-scale predictions of massive conifer mortality due to chronic temperature rise. *Nature Climate Change*, 6(3), 295–300. https://doi.org/10.1038/nclimate2873
- Miller, G. R., Chen, X., Rubin, Y., Ma, S., & Baldocchi, D. D. (2010). Groundwater uptake by woody vegetation in a semiarid oak savanna. Water Resources Research, 46(10), 1–14. https://doi. org/10.1029/2009WR008902
- Novick, K. A., Ficklin, D. L., Stoy, P. C., Williams, C. A., Bohrer, G., Oishi, A. C., Papuga, S. A., Blanken, P. D., Noormets, A., Sulman, B. N., Scott, R. L., Wang, L., & Phillips, R. P. (2016). The increasing importance of atmospheric demand for ecosystem water and carbon fluxes. Nature Climate Change, 6(11), 1023–1027. https://doi.org/10.1038/nclimate3114

- Obermeier, W. A., Lehnert, L. W., Kammann, C. I., Müller, C., Grünhage, L., Luterbacher, J., Erbs, M., Moser, G., Seibert, R., Yuan, N., & Bendix, J. (2017). Reduced CO2 fertilization effect in temperate C3 grasslands under more extreme weather conditions. *Nature Climate Change*, 7(2), 137–141. https://doi.org/10.1038/nclimate3191
- Omernik, J. M. (1987). Ecoregions of the conterminous United States.

 Annals of the Association of American Geographers, 77(1), 118–125.
- Papale, D., Reichstein, M., Aubinet, M., Canfora, E., Bernhofer, C., Kutsch, W., Longdoz, B., Rambal, S., Valentini, R., Vesala, T., & Yakir, D. (2006). Towards a standardized processing of net ecosystem exchange measured with eddy covariance technique: Algorithms and uncertainty estimation. *Biogeosciences*, 3(4), 571–583. https://doi.org/10.5194/bg-3-571-2006
- Pendergrass, A. G., Knutti, R., Lehner, F., Deser, C., & Sanderson, B. M. (2017). Precipitation variability increases in a warmer climate. Scientific Reports, 7, 17966. https://doi.org/10.1038/s41598-017-17966-y
- Porcar-Castell, A., Tyystjärvi, E., Atherton, J., van der Tol, C., Flexas, J., Pfündel, E. E., Moreno, J., Frankenberg, C., & Berry, J. A. (2014). Linking chlorophyll a fluorescence to photosynthesis for remote sensing applications: Mechanisms and challenges. *Journal of Experimental Botany*, 65(15), 4065–4095. https://doi.org/10.1093/jxb/eru191
- Poulter, B., Frank, D., Ciais, P., Myneni, R. B., Andela, N., Bi, J., Broquet, G., Canadell, J. G., Chevallier, F., Liu, Y. Y., Running, S. W., Sitch, S., & van der Werf, G. R. (2014). Contribution of semi-arid ecosystems to interannual variability of the global carbon cycle. *Nature*, 509(7502), 600–603. https://doi.org/10.1038/nature13376
- R Core Team. (2021). R: A language and environment for statistical computing. R Foundation for Statistical Computing. Retrieved from http:// www.r-project.org
- Reich, P. B., Hobbie, S. E., & Lee, T. D. (2014). Plant growth enhancement by elevated CO2 eliminated by joint water and nitrogen limitation. *Nature Geoscience*, 7(12), 920–924. https://doi.org/10.1038/ngeo2284
- Reichle, R. H., Liu, Q., Koster, R. D., Crow, W. T., De Lannoy, G. J. M., Kimball, J. S., Ardizzone, J. V., Bosch, D., Colliander, A., Cosh, M., Kolassa, J., Mahanama, S. P., Prueger, J., Starks, P., & Walker, J. P. (2019). Version 4 of the SMAP Level-4 soil moisture algorithm and data product. *Journal of Advances in Modeling Earth Systems*, 11(10), 3106–3130. https://doi.org/10.1029/2019MS001729
- Reichstein, M., Falge, E., Baldocchi, D., Papale, D., Aubinet, M., Berbigier, P., Bernhofer, C., Buchmann, N., Gilmanov, T., Granier, A., Grunwald, T., Kavrankova, K., Ilvesniemi, H., Janous, D., Knohl, A., Laurila, T., Lohila, A., Loustau, D., Matteucci, G., ... Valentini, R. (2005). On the separation of net ecosystem exchange into assimilation and ecosystem respiration: Review and improved algorithm. Global Change Biology, 11(9), 1424–1439. https://doi.org/10.1111/j.1365-2486.2005.001002.x
- Roby, M. C., Scott, R. L., & Moore, D. J. P. (2020). High vapor pressure deficit decreases the productivity and water use efficiency of rain-induced pulses in semiarid ecosystems. *Journal of Geophysical Research Biogeosciences*, 125(10), e2020JG005665. https://doi.org/10.1029/2020JG005665
- Scheiter, S., Schulte, J., Pfeiffer, M., Martens, C., Erasmus, B. F. N., & Twine, W. C. (2019). How does climate change influence the economic value of ecosystem services in savanna rangelands? *Ecological Economics*, 157, 342–356. https://doi.org/10.1016/j.ecolecon.2018.11.015
- Seneviratne, S. I., Wilhelm, M., Stanelle, T., Van Den Hurk, B., Hagemann, S., Berg, A., Cheruy, F., Higgins, M. E., Meier, A., Brovkin, V., Claussen, M., Ducharne, A., Dufresne, J.-L., Findell, K. L., Ghattas, J., Lawrence, D. M., Malyshev, S., Rummukainen, M., & Smith, B. (2013). Impact of soil moisture-climate feedbacks on CMIP5 projections: First results from the GLACE-CMIP5 experiment. Geophysical

- Research Letters, 40(19), 5212-5217. https://doi.org/10.1002/grl.50956
- Smith, W. K., Biederman, J. A., Scott, R. L., Moore, D. J. P., He, M., Kimball, J. S., Yan, D., Hudson, A., Barnes, M. L., MacBean, N., Fox, A., & Litvak, M. E. (2018). Chlorophyll fluorescence better captures seasonal and interannual gross primary productivity dynamics across dryland ecosystems of southwestern North America. *Geophysical Research Letters*, 45(2), 748–757. https://doi.org/10.1002/2017GL075922
- Smith, W. K., Dannenberg, M. P., Yan, D., Herrmann, S., Barnes, M. L., Barron-Gafford, G. A., Biederman, J., Ferrenberg, S., Fox, A. M., Hudson, A., Knowles, J. F., MacBean, N., Moore, D. J. P., Nagler, P. L., Reed, S. C., Rutherford, W. A., Scott, R. L., Wang, X., & Yang, J. (2019). Remote sensing of dryland ecosystem structure and function: Progress, challenges, and opportunities. Remote Sensing of Environment, 233, 111401. https://doi.org/10.1016/j.rse.2019.111401
- Song, C., Dannenberg, M. P., & Hwang, T. (2013). Optical remote sensing of terrestrial ecosystem primary productivity. *Progress in Physical Geography*, 37(6), 834–854. https://doi.org/10.1177/0309133313 507944
- Stocker, B. D., Zscheischler, J., Keenan, T. F., Prentice, I. C., Peñuelas, J., & Seneviratne, S. I. (2018). Quantifying soil moisture impacts on light use efficiency across biomes. *New Phytologist*, 218(4), 1430–1449. https://doi.org/10.1111/nph.15123
- Stocker, B. D., Zscheischler, J., Keenan, T. F., Prentice, I. C., Seneviratne, S. I., & Peñuelas, J. (2019). Drought impacts on terrestrial primary production underestimated by satellite monitoring. *Nature Geoscience*, 12(4), 264–270. https://doi.org/10.1038/s41561-019-0318-6
- Sulla-Menashe, D., Gray, J. M., Abercrombie, S. P., & Friedl, M. A. (2019). Hierarchical mapping of annual global land cover 2001 to present: The MODIS collection 6 land cover product. Remote Sensing of Environment, 222, 183–194. https://doi.org/10.1016/j.rse.2018.12.013
- Walker, A. P., De Kauwe, M. G., Bastos, A., Belmecheri, S., Georgiou, K., Keeling, R. F., McMahon, S. M., Medlyn, B. E., Moore, D. J. P., Norby, R. J., Zaehle, S., Anderson-Teixeira, K. J., Battipaglia, G., Brienen, R. J. W., Cabugao, K. G., Cailleret, M., Campbell, E., Canadell, J. G., Ciais, P., ... Zuidema, P. A. (2021). Integrating the evidence for a terrestrial carbon sink caused by increasing atmospheric CO2. New Phytologist, 229(5), 2413–2445. https://doi.org/10.1111/nph.16866
- Wang, X., Biederman, J. A., Knowles, J. F., Scott, R. L., Turner, A. J., Dannenberg, M. P., Köhler, P., Frankenberg, C., Litvak, M. E., Flerchinger, G. E., Law, B. E., Kwon, H., Reed, S. C., Parton, W. J., Barron-Gafford, G. A., & Smith, W. K. (2022). Satellite solar-induced chlorophyll fluorescence and near-infrared reflectance capture complementary aspects of dryland vegetation productivity dynamics. Remote Sensing of Environment, 270, 112858. https://doi.org/10.1016/j.rse.2021.112858
- Wei, Y., Liu, S., Huntzinger, D. N., Michalak, A. M., Viovy, N., Post, W. M., Schwalm, C. R., Schaefer, K., Jacobson, A. R., Lu, C., Tian, H., Ricciuto, D. M., Cook, R. B., Mao, J., & Shi, X. (2014). The north American carbon program multi-scale synthesis and terrestrial model intercomparison project part 2: Environmental driver data. Geoscientific Model Development, 7(6), 2875–2893. https://doi.org/10.5194/gmd-7-2875-2014
- Williams, A. P., Cook, E. R., Smerdon, J. E., Cook, B. I., Abatzoglou, J. T., Bolles, K., Baek, S. H., Badger, A. M., & Livneh, B. (2020). Large contribution from anthropogenic warming to an emerging north American megadrought. *Science*, 368, 314–318.
- Williams, A. P., Seager, R., Abatzoglou, J. T., Cook, B. I., Smerdon, J. E., & Cook, E. R. (2015). Contribution of anthropogenic warming to California drought during 2012–2014. Geophysical Research Letters, 42, 6819–6828. https://doi.org/10.1002/2015GL064924

- Wutzler, T., Lucas-Moffat, A., Migliavacca, M., Knauer, J., Sickel, K., Šigut, L., Menzer, O., & Reichstein, M. (2018). Basic and extensible post-processing of eddy covariance flux data with REddyProc. *Biogeosciences*, 15(16), 5015–5030. https://doi.org/10.5194/bg-15-5015-2018
- Wutzler, T., Reichstein, M., Moffat, A. M., Menzer, O., Migliavacca, M., Sickel, K., & Šigut, L. (2020). REddyProc: Post processing of (half-) hourly Eddy-covariance measurements. https://cran.r-project.org/web/packages/REddyProc
- Yan, D., Scott, R. L., Moore, D. J. P., Biederman, J. A., & Smith, W. K. (2019). Understanding the relationship between vegetation greenness and productivity across dryland ecosystems through the integration of PhenoCam, satellite, and eddy covariance data. Remote Sensing of Environment, 223, 50-62. https://doi.org/10.1016/j.rse.2018.12.029
- Yin, D., Roderick, M. L., Leech, G., Sun, F., & Huang, Y. (2014). The contribution of reduction in evaporative cooling to higher surface air temperatures during drought. *Geophysical Research Letters*, 41(22), 7891–7897. https://doi.org/10.1002/2014GL062039
- Zhang, F., Biederman, J. A., Dannenberg, M. P., Yan, D., Reed, S. C., & Smith, W. K. (2021). Five decades of observed daily precipitation reveal longer and more variable drought events across much of the western United States. *Geophysical Research Letters*, 48(7), e2020GL092293. https://doi.org/10.1029/2020GL092293
- Zhang, Y., Joiner, J., Alemohammad, S. H., Zhou, S., & Gentine, P. (2018).
 A global spatially contiguous solar-induced fluorescence (CSIF) dataset using neural networks. *Biogeosciences*, 15(19), 5779–5800. https://doi.org/10.5194/bg-15-5779-2018
- Zhang, Y., Keenan, T. F., & Zhou, S. (2021). Exacerbated drought impacts on global ecosystems due to structural overshoot. *Nature Ecology & Evolution*, 5, 1490–1498. https://doi.org/10.1038/s41559-021-01551-8
- Zhou, S., Williams, A. P., Berg, A. M., Cook, B. I., Zhang, Y., Hagemann, S., Lorenz, R., Seneviratne, S., & Gentine, P. (2019). Land-atmosphere feedbacks exacerbate concurrent soil drought and atmospheric aridity. Proceedings of the National Academy of Sciences of the United States of America, 116(38), 18848–18853. https://doi.org/10.1073/ pnas.1904955116
- Zhou, S., Zhang, Y., Williams, A. P., & Gentine, P. (2019). Projected increases in intensity, frequency, and terrestrial carbon costs of compound drought and aridity events. *Science Advances*, *5*, eaau5740. https://doi.org/10.1126/sciadv.aau5740

SUPPORTING INFORMATION

Additional supporting information may be found in the online version of the article at the publisher's website.

How to cite this article: Dannenberg, M. P., Yan, D., Barnes, M. L., Smith, W. K., Johnston, M. R., Scott, R. L., Biederman, J. A., Knowles, J. F., Wang, X., Duman, T., Litvak, M. E., Kimball, J. S., Williams, A. P., & Zhang, Y. (2022). Exceptional heat and atmospheric dryness amplified losses of primary production during the 2020 U.S. Southwest hot drought. *Global Change Biology*, 28, 4794–4806. https://doi.org/10.1111/gcb.16214